

# OVERSAMPLING IS A NECESSITY FOR RBF-COLLOCATION METHOD OF LINES

MENG CHEN\* & LEEVAN LING†

\*Department of Mathematics, Nanchang University, Nanchang, China

†Department of Mathematics, Hong Kong Baptist University, Kowloon Tong, Hong Kong

## ABSTRACT

We study a radial basis functions least-squares (RBF-LS), a.k.a. kernel-based LS, collocation method of lines [[arXiv:2109.03409](#)] for solving surface diffusion problems. Our convergence analysis requires that collocation points has to be sufficiently dense with respect to the RBF centers. In this paper, we further study how oversampling ratio, which is the numbers of collocation points over that of RBF centers for quasi-uniform sets, affects eigenvalue stability, time stepping sizes taken by Runge–Kutta methods, and accuracy.

*Keywords:* Surface diffusion, kernel-based least-squares collocation methods, partial differential equations on manifolds, eigenvalue stability.

## 1 SURFACE DIFFUSION: NOTATIONS AND PRELIMINARIES

We consider closed, connected, orientable, and complete Riemannian manifold  $\mathcal{S} \subset \mathbb{R}^d$  of dimension  $\dim \mathcal{S} := d_{\mathcal{S}} = d - 1$  and of class  $\mathcal{C}^{m+1}$ ,  $m \in \mathbb{N}$ , on which the theories in [[12, 15](#)] applied. We are interested in solving parabolic PDEs for some time-dependent surface scalar function  $u : \mathcal{S} \times [0, T] \rightarrow \mathbb{R}$  in the form of

$$\dot{u}(x, t) + \mathcal{L}_{\mathcal{S}}u(x, t) = f(x, t) \quad \text{for } (x, t) \in \mathcal{S} \times [0, T] \quad (1a)$$

$$u(x, 0) = g(x) \quad \text{for } x \in \mathcal{S}, \quad (1b)$$

for some given square integrable functions  $f : \mathcal{S} \times [0, t] \rightarrow \mathbb{R}$  and  $g : \mathcal{S} \rightarrow \mathbb{R}$ , and second-order uniformly elliptic operator in divergence form

$$\mathcal{L}_{\mathcal{S}}u(x, t) := -\nabla_{\mathcal{S}} \cdot (A(x, t)\nabla_{\mathcal{S}}u(x, t)) + bu(x, t) \quad \text{for } (x, t) \in \mathcal{S} \times [0, T], \quad (2)$$

where  $b$  is a constant, and the symmetric surface intrinsic diffusion tensor  $A : \mathcal{S} \times [0, t] \rightarrow \mathbb{R}^{d \times d}$  satisfies, for all  $x \in \mathcal{S}$  and  $t \in [0, T]$ , some symmetric positive definiteness assumption [[2](#), Asm. 1] when restricted to the tangent space  $\mathcal{T}_x\mathcal{S}$  of  $\mathcal{S}$  at  $x \in \mathcal{S}$ . The surface diffusion operator (2) is defined by a smooth vector field  $\mathbf{n} : \mathcal{S} \rightarrow \mathbb{R}^d$  that spans the normal space and the  $\mathcal{T}_x\mathcal{S}$ -orthogonal projection matrix

$$P(x) := I_d - \mathbf{n}(x)\mathbf{n}(x)^T. \quad (3)$$

Then, the surface gradient operator  $\nabla_{\mathcal{S}}$

$$\nabla_{\mathcal{S}}v(x) := P(x)\nabla(v \circ \text{cp})(x) = \nabla(v \circ \text{cp})(x), \quad x \in \mathcal{S}, \quad (4)$$

and surface divergence operator  $\nabla_{\mathcal{S}} \cdot$

$$\nabla_{\mathcal{S}} \cdot g(x) := (P(x)\nabla) \cdot (g \circ \text{cp})(x) = \nabla \cdot (g \circ \text{cp})(x), \quad x \in \mathcal{S}, \quad (5)$$

are defined, respectively, for continuously differentiable scalar surface function  $v : \mathcal{S} \rightarrow \mathbb{R}$  and for continuously differentiable surface vector field  $g : \mathcal{S} \rightarrow \mathbb{R}^d$ . In (4) and (5)  $\text{cp}(x)$  is the  $\mathcal{C}^m$ -smooth Euclidean closest point retraction map:

$$\text{cp}(y) := \arg \inf_{x \in \mathcal{S}} \|x - y\|_{L^2(\mathbb{R}^d)} : \Omega \rightarrow \mathcal{S}, \quad (6)$$

in some narrow-band domain  $\Omega$  containing  $\mathcal{S}$ .

## 2 RBF-COLLOCATION METHOD OF LINES

In [10, 11, 24], spherical RBF approximation methods with MOL were applied to solving parabolic PDEs on unit spheres. Backward Euler and Crank-Nicolson schemes were respectively employed in [10] with meshless collocation approach on fixed surfaces, and in [11] with collocation and other two (Galerkin and RBF-FD) methods on evolving spheres. The authors of [24] used Laplace transforms and quadrature in time and Galerkin approximation in space.

We skip the semi-discretize solution and present the fully discretize RBF-collocation method of lines in [2] with the minimal set of notations. First, we pick a global, symmetric positive definite, and Sobolev space  $H^{m+1/2}(\mathbb{R}^d)$  reproducing [17] kernels  $\Psi = \Psi_{m+1/2} : \mathbb{R}^d \times \mathbb{R}^d \rightarrow \mathbb{R}$  to  $\mathcal{S}$ , whose Fourier transforms decay like

$$c_1(1 + \|\omega\|_2^2)^{-(m+1/2)} \leq \hat{\Psi}(\omega) \leq c_2(1 + \|\omega\|_2^2)^{-(m+1/2)} \quad \text{for all } \omega \in \mathbb{R}^d, \quad (7)$$

for some constants  $0 < c_1 \leq c_2$ ; for example, we can use the standard Whittle-Matérn-Sobolev kernels [17] or the Wendland compactly supported kernels [23] with smoothness order  $m + 1/2$ . The extra half order of smoothness in  $\Psi$  ensures that the corresponding restricted surface kernel reproduces  $H^m(\mathcal{S})$  [8, 18].

For some set of  $n_Z$  trial centers  $Z = \{z_1, \dots, z_{n_Z}\} \subset \mathcal{S}$  with fill distance  $h_Z$  and the separation distance  $q_Z$

$$h_Z := \sup_{\zeta \in \mathcal{S}} \inf_{\eta \in Z} \text{dist}(\zeta, \eta) \quad \text{and} \quad q_Z := \frac{1}{2} \inf_{z_i \neq z_j \in Z} \text{dist}(z_i, z_j), \quad (8)$$

we define the RBF trial space by

$$\mathcal{U}_{Z,\mathcal{S},\Psi} := \text{span}\{\Psi(\cdot, z_j) \mid z_j \in Z\}. \quad (9)$$

We assume that  $Z$  is quasi-uniform with bounded mesh ratio  $\rho_Z = h_Z/q_Z \geq 1$  as  $Z$  is being refined. We seek time-dependent numerical solution to surface diffusion (1) in the trial space with a set of unknown coefficient functions of time  $\lambda_Z(t) := [\lambda_1(t), \dots, \lambda_{n_Z}(t)]^T$ , that is,

$$u_Z(\cdot, t) = \sum_{z_j \in Z}^{n_Z} \lambda_j(t) \Psi(\cdot, z_j) =: \Psi(\cdot, Z) \lambda_Z(t). \quad (10)$$

Putting ansatz (10) into the governing equation (1a) and collocating, a.k.a oversampling, at some sufficiently dense set of quasi-uniform collocation points  $X = \{x_1, \dots, x_{n_X}\} \subset \mathcal{S}$  satisfying the following the denseness constraints [2, Lem. 3.5]

$$\begin{cases} Ch_X^{2m-4} h_Z^{-2m} < \frac{1}{4} & \text{if } h_Z \leq 1, \\ Ch_X^{2m-4} h_Z^{-2m+4} < \frac{1}{4} & \text{otherwise,} \end{cases} \quad (11)$$

for some  $C$  depending on  $\Psi, \mathcal{S}, \mathcal{L}, \rho_Z$  and  $\rho_X$  yields overdetermined differential algebraic equations (DAE)

$$[\Psi(X, Z)] \dot{\lambda}_Z(t) + [\mathcal{L}_\mathcal{S} \Psi(X, Z)] \lambda_Z(t) = f(X, t), \quad (12)$$

where the  $ij$ -entry of the  $n_X \times n_Z$  matrix  $[\Psi(X, Z)]$  (and  $[\mathcal{L}_\mathcal{S} \Psi(X, Z)]$ ) is defined by  $\Psi(x_i, z_j)$  (and  $\mathcal{L}_\mathcal{S} \Psi(x_i, z_j)$ ) for  $x_i \in X$  and  $z_j \in Z$ . Instead of coefficient functions, one may wish to work with nodal values  $u_Z(t)$  of  $u$  at  $Z$  by considering

$$[\Psi(X, Z) \Psi(Z, Z)^{-1}] \dot{u}_Z(t) + [\mathcal{L}_\mathcal{S} \Psi(X, Z) \Psi(Z, Z)^{-1}] u_Z(t) = f(X, t). \quad (13)$$

Let  $\dagger$  be the pseudoinverse operator. We define the numerical solution in the form of (10) with coefficient functions  $\lambda_Z \in (C^{p+1}[0, T])^{n_Z}$  that solve the  $n_Z \times n_Z$  ODE system

$$\dot{\lambda}_Z(t) = [-\Psi(X, Z) \dagger \mathcal{L}_\mathcal{S} \Psi(X, Z)] \lambda_Z(t) + \Psi(X, Z) \dagger f(X, t), \quad (14)$$

or nodal values that solve

$$\dot{u}_Z(t) = [-\Psi(Z, Z) \Psi(X, Z) \dagger \mathcal{L}_\mathcal{S} \Psi(X, Z) \Psi(Z, Z)^{-1}] u_Z(t) + \Psi(Z, Z) \Psi(X, Z) \dagger f(X, t), \quad (15)$$

subject to any initial condition  $\lambda_Z(0)$  (or  $u_Z(0)$ ) that enjoys  $H^1(\mathcal{S})$ -convergence, i.e., simply the interpolant of initial condition  $g$  in (1b) from the trial space  $\mathcal{U}_{Z,\mathcal{S},\Psi}$ .

If we define numerical solution  $u_{Z,\alpha}$  to the PDE solution  $u^*$  by the solution of surface diffusion problem as in (14) with  $b = 0$  and using a regularized least-squares approximation in [2, Sect. 3.4] as initial condition  $\lambda_{Z,\alpha}(0)$  with regularization parameter  $0 \leq \alpha < h_X^{m-d_S/2}$ , then the following estimate holds

$$\begin{aligned} \mathcal{E}(u_{Z,\alpha} - u^*) \leq & C \left( h_Z^{2m-4-d_S} (\|\dot{u}^*\|_{H^{m-2}(\mathcal{S})}^2 + \|u^*\|_{H^m(\mathcal{S})}^2) \right. \\ & \left. + (h_Z^{2m-2} + h_X^{-2} h_Z^{2m-d_S} + h_X^{2m-2}) \|u^*(\cdot, 0)\|_{H^m(\mathcal{S})}^2 \right) \end{aligned}$$

with error functional

$$\mathcal{E}(u) := \operatorname{ess\,sup}_{0 \leq t \leq T} \|u\|_{H^1(\mathcal{S})}^2 + \|u\|_{L^2(0,T;H^1(\mathcal{S}))}^2 + \|\dot{u}\|_{L^2(0,T;H^0(\mathcal{S}))}^2, \quad (16)$$

see [2, Thm. 3.6 & Cor. 4.2]. We end this methodology section with a few remarks. First of all, Computation of the entries in  $[\mathcal{L}_S \Psi(X, Z)]$  can be done in different ways:

1. If we know the normal vector  $\mathbf{n}$  of  $\mathcal{S}$  analytically, then  $\mathcal{L}_S \Psi$  can be symbolically obtained by using the formulas (4) and (5).
2. If  $\mathbf{n}$  is known pointwise in some oriented point cloud of  $\mathcal{S}$ , then a pseudospectral RBF approximation [3, 9] can be used to approximate  $\mathcal{L}_S \Psi$  at any point in the point cloud.
3. If  $\mathcal{S}$  were implicitly defined by some discrete point sets, then we first estimate all necessary normal vectors by some kernel interpolation level-set approach [7, 16]; return to Case 2.

In our numerical experiments, we consider surfaces with parametric equations so that have normal vector  $\mathbf{n}$  analytically.

Next, the ODE matrices in (14) and (15) are similar and share the same eigenvalues; we only consider the former in numerical studies. In our implementation, ODE (14) with a pseudoinverse matrix is not used. Instead, we compute the reduced QR-factorization of the  $n_X \times n_Z$  matrix  $[\Psi(X, Z)] =: QR$ , where  $Q$  is  $n_X \times n_Z$  and  $R$  is square. Then, we solve

$$R \dot{\lambda}_Z(t) = [-Q^T \mathcal{L}_S \Psi(X, Z)] \lambda_Z(t) + Q^T f(X, t), \quad (17)$$

with mass matrix  $R$  that can be solved by many black-box ODE solvers; in our cases, we use the explicit ODE45 Runge–Kutta method in MATLAB.

### 3 OVERSAMPLING VS EIGENVALUE STABILITY

Using least-squares in RBF interpolation [1] and with method of lines were numerically shown to be beneficial [20] over a decade ago. Convergence of least-squares RBF collocation method for elliptic PDEs can also be proven recently [5]. Yet, oversampling is not a standard in RBF method of lines, for example, we see  $Z = X$  for example in [6, 10, 11, 13]. In such

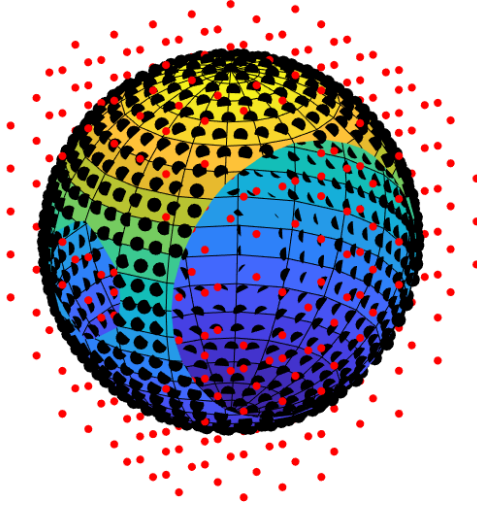


Figure 1: Exmp. 3.1–3.2: Schematic demonstration of data point distributions. (Black) Quasi-uniform data points on the unit sphere, and (Red) Regular grid in some narrow band domain containing the unit sphere.

square cases, the DAE in (12) become a system of ODEs with symmetric positive definite mass matrix  $\Psi(Z, Z)$ . Published results are, of course, the successful cases and it is hard to draw conclusion from them about the necessity of oversampling.

The rest of this paper contains numerical experiments aiming to identify some appropriate range (if needed at all) of oversampling ratio  $n_X/n_Z$  numerically that yield stable eigenvalues. This work provides a rule-of-thumb to setup the theoretically-proven convergent RBF-collocation method of lines in Section 2 from practical uses. In all examples below, we use the  $H^{m+1/2}(\mathbb{R}^d)$ -reproducing Sobolev kernel defined using the Bessel functions of the second kind  $\mathcal{K}$  as

$$\Psi_{m+1/2}(x, z) := \|x - z\|_{\ell^2(\mathbb{R}^d)}^{(m+1/2)-d/2} \mathcal{K}_{(m+1/2)-d/2}(\|x - z\|_{\ell^2(\mathbb{R}^d)}) \quad \text{for } x, z \in \mathbb{R}^d$$

with on-surface smoothness order  $m > (d - 1)/2$  in dimension  $d = 3$ .

**Example 3.1. Isotropic diffusion-reaction on the unit sphere.**

We consider the surface PDE  $\dot{u} - \Delta_S u + 3u = f$  on the unit sphere. We generate\* sets

$$n_Z \in \{658, 1266, 2506, 3850\} \tag{18}$$

of quasi-uniform RBF centers  $Z \subset \mathcal{S}$ , see the on-surface black dots in Figure 1 for a schematic demonstration. The irregular pattern in the tested  $n_Z$  is for the sake of comparison

---

\*<https://www.mathworks.com/matlabcentral/fileexchange/6977-pointonsphere>

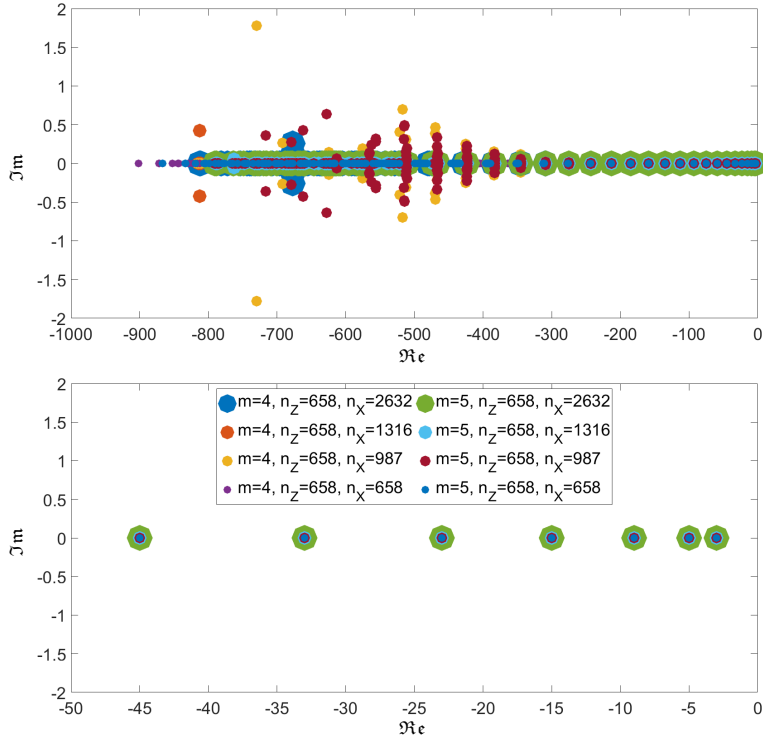


Figure 2: Exmp. 3.1: We observe stable eigenvalues in  $\mathbb{C}$  when both the kernel order of smoothness  $m$  and the number of RBF centers  $n_Z$  are relative small; oversampling does not have any obvious effect in terms of eigenvalue distribution. The provided legend applies to both subfigures: (TOP) full spectra, and (BOTTOM) Zoom-in near the origin.

the next example. Now, for oversampling ratio

$$n_X/n_Z \in \{1, 1.5, 2, 4\},$$

sets of  $n_X$  collocation points were generated similarly for each tested set  $Z$ . We compute all eigenvalues of the ODE matrix  $[-\Psi(X, Z)^\dagger \mathcal{L}_S \Psi(X, Z)]$  in (14) with the sets of  $X, Z$  we constructed just now and present readers a summary of observations.

**Observation 1:** *Oversampling is not needed in cases of small  $m$ .*

In Figure 2, we show eigenvalue distributions corresponding the ODE matrices with the smallest  $n_Z = 658$  RBF centers and smoothness order  $m = 4$  and  $5$ , which were selected due to their stable eigenvalues. From the top figure, we could barely observe that higher ratio of oversampling (see larger markers in figure) can reduce the spectral radius and also results in eigenvalues closer to the real number line. Zooming-in towards the origin in the bottom figure, we can see that all eight test cases can well approximate the largest eigenvalues.

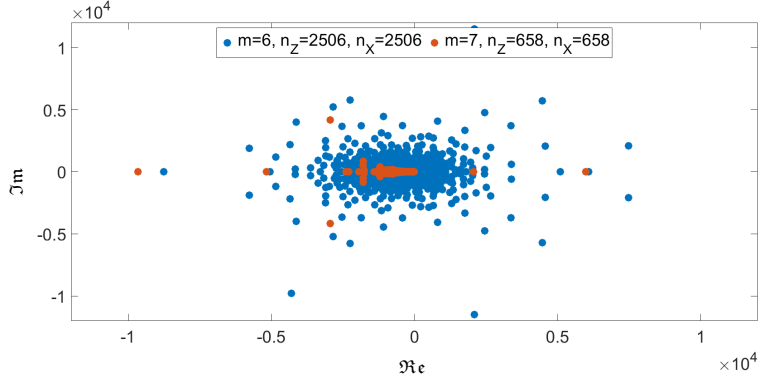


Figure 3: Exmp. 3.1: RBF method of lines without any oversampling has unstable eigenvalues when either  $m$  and/or  $n_Z$  increases.

Observation 2: *Eigenvalues become unstable if either  $m$  or  $n_Z$  increases.*

A fact without providing evidence is that, for  $m = 6$ , eigenvalues are stable for both  $n_X = n_Z = 658$  and  $1266$  without oversampling. Keeping  $m = 6$  fixed and increase number of RBF centers to  $n_Z = 2506$  brings instability into the eigenvalue distributions, see blue markers in Figure 3. Now, if we keep  $n_Z = 658$  fixed as in Figure 2 but increase the smoothness order to  $m = 7$ , we see unstable eigenvalues once more (see orange markers in figure). The message is that RBF method of lines without oversampling does not allow  $m$ -nor  $n_Z$ -convergence.

Observation 3: *Stability in eigenvalues can be regained by oversampling.*

For all tested  $n_Z$ , we use  $n_X = 1.5n_Z$  to generate the collocation points  $X$ . In Figure 4, eigenvalues obtained with  $m = 6, 8, 10$  were shown;  $m = 7, 9$  were omitted due to the high similarity. By comparing with the top of Figure 2, we see that the spectra in this example lie in a smaller range. Yet, the most obvious and important difference is the spurious zero eigenvalue we can clear see in the bottom subfigure. We reported that all 12 tested cases here contain zero eigenvalue with different multiplicity, which depends on  $m$ . This is the problem of ill-conditioning in RBF methods (using standard RBF basis functions); the kernel matrix  $[\Psi(X, Z)]$  eventually becomes rank deficient as we increase the order  $m$  and/or the number of points in  $Z$ . So, as we push the RBF approximation power to its finite-precision limit, the ODE in (17) will unavoidably become DAE. Schaback's uncertainty principle [22] for interpolation and the folklore for time-independent PDEs both says that we should tune the RBFs to yield nearly singular kernel/PDE matrices under the given computational precision. Should we do the same here to RBF method of lines?

Observation 4: *Zero eigenvalue is not a problem, and DAE seems to be better than ODE.*

Let  $u^*(x, t) = \exp(x_1 + 1/(1+t))$  for  $x = (x_1, x_2, x_3) \in \mathcal{S}$  and  $t \in [0, 1]$  be the solution to our target PDE. We compute the corresponding source function  $f := \partial_t u^* - \Delta_{\mathcal{S}} u^* + 3u^*$  analytically. Then, we finish setting up the ODE (17) using a fixed  $Z$  with

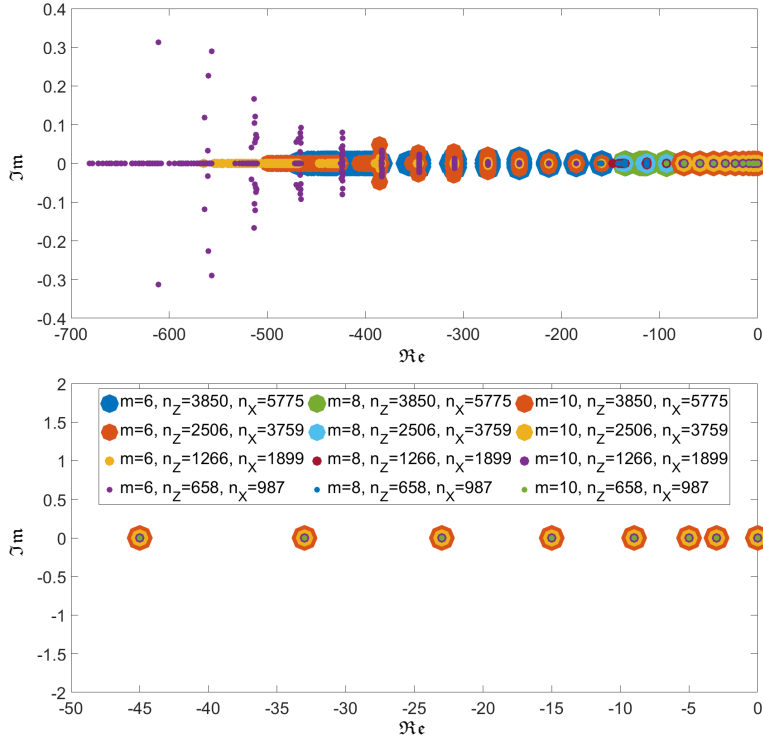


Figure 4: Exmp. 3.1: By imposing  $1.5\times$  oversampling ratio, we consistently observe stable eigenvalues in  $\mathbb{C}$  when using kernel with high order of smoothness  $m$  and more RBF centers. The provided legend applies to both subfigures: (TOP) full spectra, and (BOTTOM) Zoom-in near the origin and note the spurious zero eigenvalue.

$n_Z = 658$ , but various kernel smoothness and oversampling ratios. All ODEs (in which some are indeed DAEs because of the previous observation) are then solved by ODE45 in MATLAB without fine-tuning any error tolerances. Representative results were overloaded in Figure 5, which we shall clearly walk through the details.

The top subfigure of Figure 5 shows the cumulative time of the time-stepping in ODE45. Note that, due to the adaptivity in time-stepping, some of these curves are not straight lines, see the earlier steps in particular. The two steepest curves, that come from  $m = 8$ , and  $n_X = 987$  and  $2632$ , are the winner in terms of numbers of time-stepping needed to complete the time integration. Since all ODE matrices in (17) are of the same size, fewer time steps can almost translate into a faster overall PDE solving time. The extra cost of using different  $n_X > n_Z$  is due to the computation of reduced QR in (17) that grows linearly and quadratically with respect to  $n_X$  and  $n_Z$ , [14, Tab. 3.1]. The outlier on the other end also comes from  $m = 8$  but without oversampling. This is a fail setup with unstable eigenvalue, and ODE45 runs with very small time-step trying to solve this stiff problem. Numerical



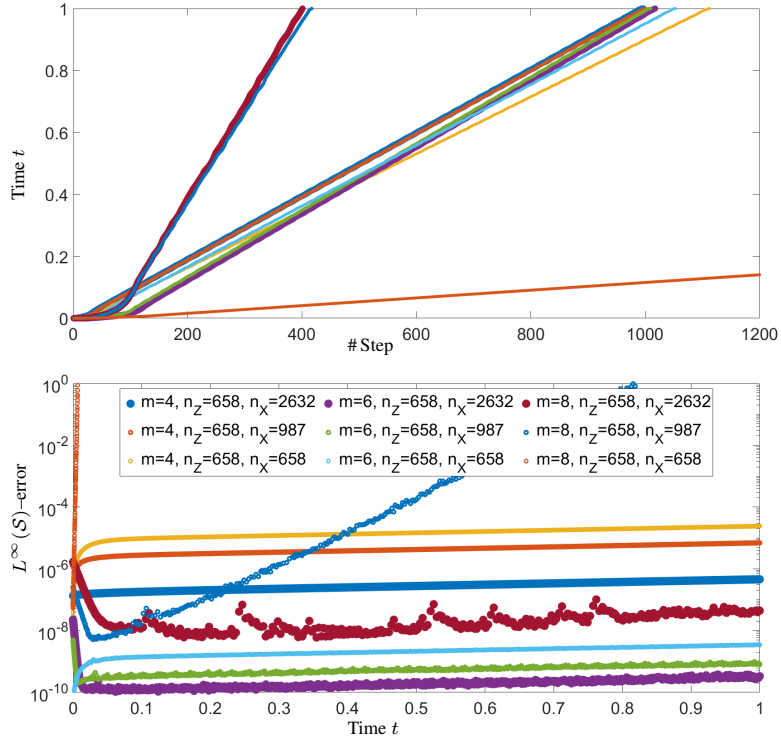


Figure 5: Exmp. 3.1: Summaries of ODE45 results. (TOP) Current time against the number of adaptive time steps, (BOTTOM) maximum errors of various RBF method of lines solutions against time.

$n_X$	$m = 4$		$m = 5$		$m = 6$		$m = 7$		$m = 8$	
	$\kappa$	Err	$\kappa$	Err	$\kappa$	Err	$\kappa$	Err	$\kappa$	Err.
658	5e9	2.4e-5	1e12	3.0e-7	6e14	3.4e-9	6e18	NaN	6e19	NaN
987	8e9	6.9e-6	2e12	8.2e-8	8e14	8.0e-10	1e17	7.6e-10	2e17	8.1e+1
256	8e9	9.5e-7	2e12	1.3e-8	8e14	3.1e-10	1e17	8.0e-10	1e17	2.4e-4
2632	8e9	4.6e-7	2e12	1.1e-8	8e14	3.3e-10	9e16	8.1e-10	1e17	4.4e-8

Table 1: Exmp. 3.1: With  $n_Z = 658$  fixed, the condition number ( $\kappa$ ) of the kernel matrix  $\Psi(X, Z)$  and final  $L^\infty(S)$ -error of the RBF method of lines solution at the final time  $t = 1$ .

garbage will be the end product after a long runtime. The group of curves in the middle are results from  $m = 4$  and 6 with all tested oversampling ratios.

We move on the bottom of Figure 5 and study the accuracy of numerical solutions obtained from RBF method of lines. From smallest to largest error at  $t = 0.1$ , we see that

- three  $m = 6$  error curves (in colors purple, green, and sky blue) have the smallest error,
- two  $m = 8$  error curves (in colors red and cobalt) comes next,

- three  $m = 4$  error curves (in color blue, orange, and yellow) are also convergent,
- $m = 8$  without oversampling blows the error up immediately.

Let us also take the number of zero eigenvalues in the kernel matrix  $\Psi(X, Z)$ , instead of the ODE matrix of (14), listed in Table 1 into account. When  $m = 4$ , there is no zero eigenvalue in the kernel matrix  $\Psi(X, Z)$ . Based on the information in Figure 2, the ODE matrix is also full rank and we are dealing with ODEs. On the other hands, we are working with DAE when  $m = 6$  and 8 subject to different degree of rank loss in the ODE matrix. Recall their eigenvalue distribution in Figure 4.

We see that least error in Table 1 occur when  $\kappa(\Psi(X, Z)) \lesssim 1/\varepsilon_{\text{machine}}$ . So the uncertainty principle remains helpful in selecting smoothness order  $m$ . Yet, indicators for the selection of  $n_X$  remain missing. From the last column ( $m = 8$ ) of the table, we see that solution accuracy heavily depends on the oversampling ratio. Yet, ranks and condition numbers of all three ( $987 \leq n_X \leq 2632$ ) ODE matrices  $[-\Psi(X, Z)^\dagger \mathcal{L}_S \Psi(X, Z)]$  are 121 and  $\mathcal{O}(1e17)$ .

**Example 3.2.** *Using regular RBF centers  $Z$  in some narrow band domain  $\Omega \supset \mathcal{S}$ .*

Given the same number  $n_Z$  of RBF centers, we can maximize the minimum separating distance  $q_Z$  of  $Z$  if we can place  $Z$  out-of-surface. Before proceeding, we emphasize that our convergence theory in [2] does not apply, although this is the data point structure used in embedding methods [4, 19, 21].

For some small parameter  $\delta$ , let the narrow band domain be

$$\Omega := \Omega_{\delta, \mathcal{S}} = \left\{ x \in \mathbb{R}^d : \|x - z\|_2 \leq \delta \text{ for some } z \in \mathcal{S} \right\}.$$

We define set of near-surface regular RBF centers by  $Z := (\delta \mathbb{W})^d \cap \Omega$ . Using four values of  $\delta$  between 0.125 to 0.25, we can obtain sets of  $Z$  with exactly  $n_Z$  points as in (18) in Exmp. 3.1, see red dots in Figure 1. Collocation points  $X$  must lie on the surface and they are generated as in the previous example.

In Figure 6, we see from the top subfigure that, without oversampling, unstable eigenvalues of the ODE matrices appear in all tested values of  $m$ , including  $m = 4, 5$  that works fine in the previous example with  $Z \subset \mathcal{S}$ . In the bottom subfigure, oversampling can greatly stabilize the eigenvalue distribution.

Now we turn to Table 2 and note that  $m = 6$  is still the optimal order of kernel smoothness. We also observe that the error profiles for  $m = 7, 8$  here behave very much like  $m = 8$  in the previous example. In all cases, the  $n_X$ -convergence behaviours are pronounced.

**Example 3.3.** *Anisotropic diffusion with non-identity diffusion tensor  $A$  in (2).*

In this example, we considered a more complicated setup. Firstly, we consider a dupin cyclide, see Figure 7, on which  $n_Z = 314, 744, 1320$  RBF centers and  $n_X = 2976, 5296$  collocation points were placed quasi-uniformly. We only consider Sobolev kernels with smoothness  $m = 6$ .

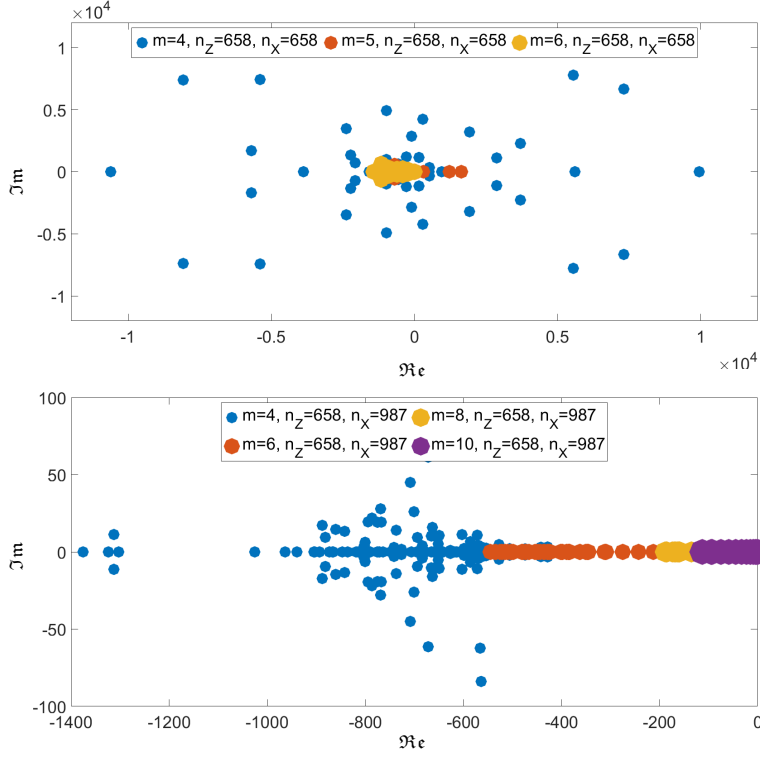


Figure 6: Exmp. 3.2: When we place RBF centers in a narrow band domain containing  $\mathcal{S}$ , (TOP) square approach with  $X = Z$  yields unstable eigenvalues for all tested smoothness orders  $m$ , and (BOTTOM) imposing  $1.5\times$  oversampling ratio is sufficient for stable eigenvalues.

$n_X$	$m = 4$		$m = 5$		$m = 6$		$m = 7$		$m = 8$	
	$\kappa$	Err	$\kappa$	Err	$\kappa$	Err	$\kappa$	Err	$\kappa$	Err
658	2e19	NaN	3e19	NaN	1e19	NaN	3e19	NaN	4e19	NaN
987	2e12	2.6e-6	3e14	1.5e-7	1e17	8.3e-9	2e17	9.4e-1	3e17	1.4e-1
256	1e12	2.4e-6	3e14	1.5e-7	7e16	7.2e-9	2e17	6.3e-5	2e17	1.1e-5
2632	1e12	2.5e-6	3e14	1.5e-7	6e16	7.4e-9	1e17	7.8e-8	1e17	1.2e-8

Table 2: Exmp. 3.2: Results corresponding to Table 1 for near-surface regular RBF center in a narrow band domain.

For PDEs, we consider differential operator (2) with  $b = 3$  an non-identity time-independent diffusion tensor

$$A(x, t) := P(x) \text{diag}([1 + x_1^2, 1, 1]),$$

where  $P$  is the projection matrix in (3) so that the matrix  $A(x, t) : \mathcal{T}_x\mathcal{S} \rightarrow \mathcal{T}_x\mathcal{S}$  is symmetric positive definite on the tangent space  $\mathcal{T}_x\mathcal{S}$  of  $\mathcal{S}$ . We show all error profiles at time  $t = 1$  in

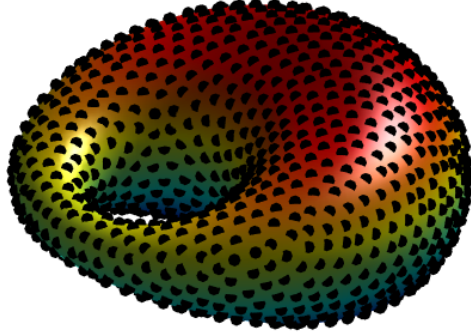


Figure 7: Exmp. 3.3: Schematic demonstration of quasi-uniform data point distributions on a Dupin Cyclide.

$n_Z \setminus n_X$	744	1320	2976	5296
314	1.29e-5 ( 789)	1.32e-5 ( 789)	1.19e-5 ( 757)	8.63e-6 ( 793)
744	NaN	<b>8.98e-6 (1333)</b>	<b>8.91e-6 (1249)</b>	2.80e-6 (1145)
1320	NaN	NaN	8.88e-6 (2457)	<b>2.61e-6 (2497)</b>

Table 3: Exmp. 3.3: Maximum errors at  $t = 1$  (and number of ODE45 time steps taken) of the solutions in Figure 8, see last two columns.

Figure 8. For a very small  $n_Z = 314$  of RBF centers, we see in the first row that  $9.4\times$  and  $16.8\times$  oversampling yields no improvement in accuracy. Indeed, the (omitted) error profile of  $(n_Z, n_X) = (314, 744)$  also show similar error pattern.

If we read Figure 8 top-down, we can see that errors for  $n_X = 2976$  in the first column cease improve as  $n_Z$  increases. Whereas, in the second column, errors keep reducing as RBF centers were refined. Yet, a more fair comparison is to do so diagonally, i.e., we compare

- $(n_Z, n_X) = (314, 2976)$  and  $(744, 5296)$  with similar oversampling ratios of  $9.5\times$  and  $7.1\times$  respectively, and
- $(n_Z, n_X) = (744, 2976)$  and  $(1320, 5296)$  both with oversampling ratios  $4.0\times$ , see boldfaced entries in Table 3.

In both cases, the reduction in error is trivial. We point out the final accuracy is limited by the ODE45 tolerance; all entries in Table 3 are all rather accurate and, hence, are not suitable for estimating the convergence rate of the RBF method of lines.

To get some intuitions on computational time, we show in Figure 9 the numbers of time steps ODE45 required to get the job done. In contrast to the fixed  $n_Z$  in Figure 5, we are now seeing results associated with different values of  $n_Z$ . This figure is easy to summarize: larger  $n_Z$  requires more smaller time steps in ODE45, which suggests that the ODE system (17) is getting stiff with increasing  $n_Z$ .

**Example 3.4. Simulating a surface diffusion.**

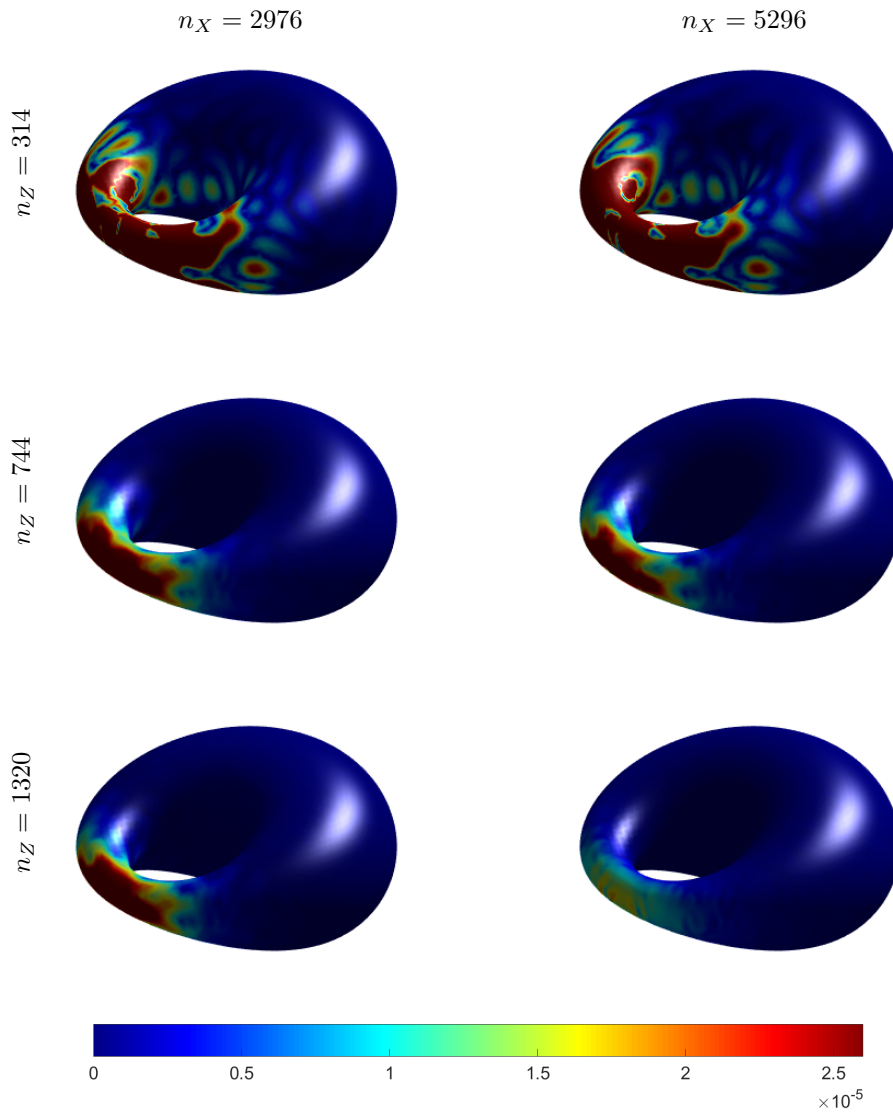


Figure 8: Exmp. 3.3: Error profiles, which use the same colormap for easy comparison, of the RBF method of lines solutions to an anisotropic diffusion reaction equation for various numbers of RBF centers  $n_Z$  (down the rows) and collocation points  $n_Z$  (across the columns).

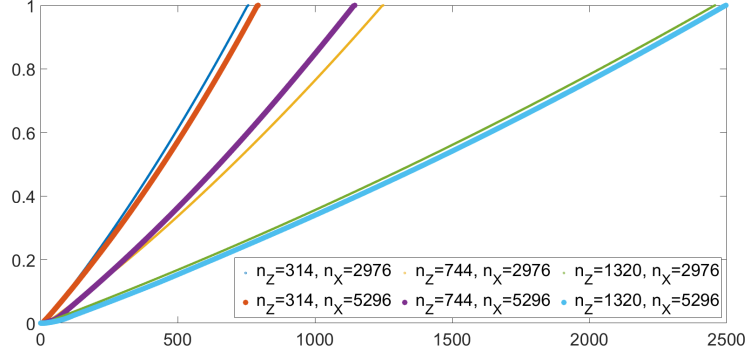


Figure 9: Exmp. 3.3: Current time against the number of adaptive time steps to complete the integration process in finding solutions in Figure 8.

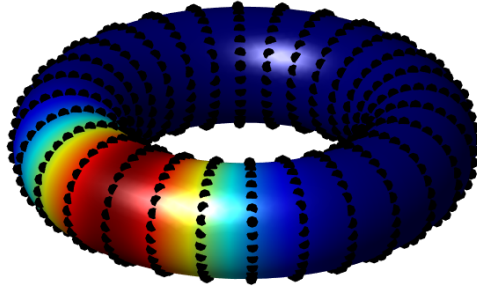


Figure 10: Exmp. 3.4: Schematic demonstration of data point distributions on Torus with values of the source function  $f$  as colormap.

In this last example, we want to simulate some simple physics. We consider a surface diffusion  $\mathcal{L}_S = -\Delta_S$  in (2) for  $t \in [0, 10]$  on a Torus<sup>†</sup>, on which we can parametrized  $(x_1, x_2, x_3) \in \mathcal{S}$  by

$$\begin{aligned} x_1 &= \left(1 + \frac{1}{3} \cos(\theta)\right) \cos(\phi), \\ x_2 &= \left(1 + \frac{1}{3} \cos(\theta)\right) \sin(\phi), \\ x_3 &= \frac{1}{3} \sin(\theta), \end{aligned}$$

for  $\theta, \phi \in [-\pi, \pi]$ . We use zero initial condition  $g = 0$  and the right-handed side function  $f(\theta, \phi) = \exp(-3\phi^2)$ , see Figure 10.

<sup>†</sup>Torus:  $x^2 + y^2 + z^2 + 1^2 - (1/3)^2 = 0$

Based on the results in Table 3, using  $(n_Z, n_X) = (744, 1320)$  is the overall winner in terms of both accuracy and computation time (measured by ODE45 steps). We generate  $n_Z = 784$  RBF centers and  $n_X = 1156$  collocation points using the above parametric equation, see points distribution in Figure 10. The mesh ratios of data points in this example is larger than those in the previous examples. We again apply ODE45 to finish solving the PDE. A few snapshots of the numerical solution were given in Figure 11, from which we can see the correct physics of heat diffusion from a localized source. We do not have an analytic solution in hand to compute errors. But we can report that increasing  $n_X$  does not result in any recognizable difference in solutions.

#### 4 CONCLUSION

We perform numerical experiments to study the effect of oversampling, i.e., using more collocation points than RBF centers, in RBF method of lines. All the provided tests were solved by MATLAB function ODE45, which is the bottleneck of the final accuracy. Instead of targeting high order convergence, we are more interested in the eigenvalue stability in the ODE system after spatial discretization by RBF. We observe that oversampling is a must if users either employ kernels with high smoothness or uses more RBF basis in the numerical solution. It is also observed that the number of step ODE45 needed increases with the number of RBF centers, but not collocation points. The most computational efficient setup is to use enough RBF centers, which can be selected by Schaback’s uncertain principle, to reach the ODE45 temporal error tolerance and use oversampling, say  $2\times$ . We successfully run a simulation based on this rule-of-thumb without fine tuning.

#### ACKNOWLEDGEMENTS

This work was supported by the Hong Kong Research Grant Council GRF Grants, National Natural Science Foundation (Grant No. 12001261) and Jiangxi Provincial Natural Science Foundation (Grant No. 20212BAB211020).

#### REFERENCES

- [1] M. D. Buhmann, Radial basis functions: Theory and implementations, vol. 12 of Cambridge Monographs on Applied and Computational Mathematics, Cambridge University Press, Cambridge, 2003.
- [2] M. Chen, K. C. Cheung, L. Ling, A kernel-based least-squares collocation method for surface diffusion, arXiv: 2109.03409 [math.NA] (2021).
- [3] M. Chen, L. Ling, Extrinsic meshless collocation methods for PDEs on manifolds, SIAM J. Num. Anal. 58 (2) (2020) 988–1007.
- [4] K. C. Cheung, L. Ling, A kernel-based embedding method and convergence analysis for surfaces PDEs, SIAM J. Sci. Comput. 40 (1) (2018) A266–A287.
- [5] K. C. Cheung, L. Ling, R. Schaback,  $\mathcal{H}^2$ -convergence of least-squares kernel collocation methods, SIAM J. Numer. Anal. 56 (1) (2018) 614–633.

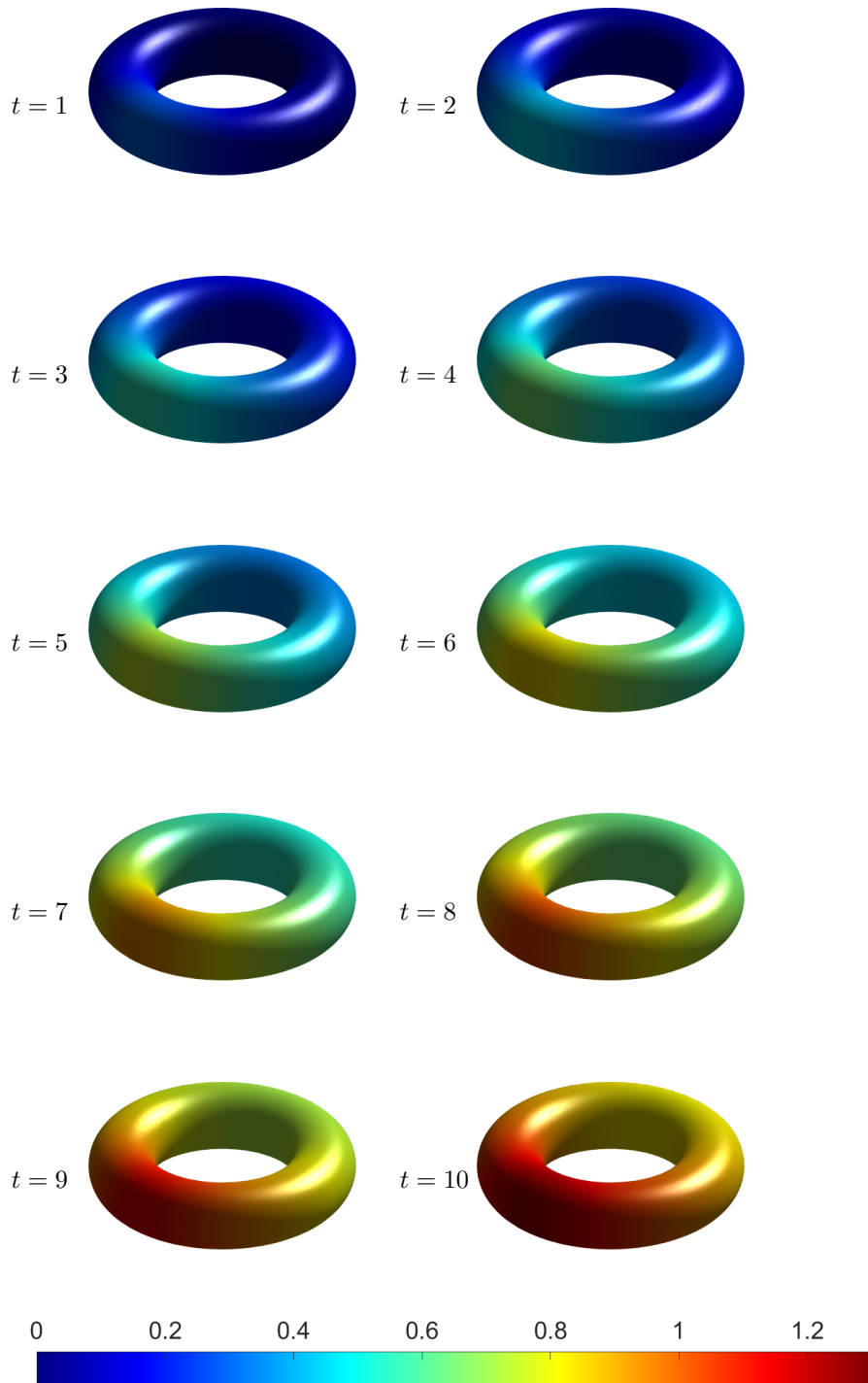


Figure 11: Exmp. 3.4: With  $n_Z = 784$  and  $n_X = 1156$ , snapshots profiles, which use the same colormap for easy comparison, of the RBF method of lines solutions to an isotropic diffusion reaction equation at various time steps for  $m = 6$ .



- [6] Y. Dereli, The meshless kernel-based method of lines for the numerical solution of the nonlinear Schrödinger equation, *Eng. Anal. Bound. Elem.* 36 (9) (2012) 1416–1423.
- [7] N. Flyer, B. Fornberg, V. Bayona, G. A. Barnett, On the role of polynomials in RBF-FD approximations: I. interpolation and accuracy, *J. Comput. Phys.* 321 (2016) 21 – 38.
- [8] E. Fuselier, G. B. Wright, Scattered data interpolant on embedded submanifolds with restricted positive definite kernels: Sobolev error estimates, *SIAM J. Numer. Anal.* 50 (3) (2012) 1753–1776.
- [9] E. J. Fuselier, G. B. Wright, A high-order kernel method for diffusion and reaction-diffusion equations on surfaces, *J. Sci. Comput.* 56 (2013) 535–565.
- [10] Q. Gia, Approximation of parabolic pdes on spheres using spherical basis functions, *Adv. Comput. Math.* 22 (4) (2005) 377–397.
- [11] Q. T. L. Gia, W. Mclean, Solving parabolic equations on the unit sphere via laplace transforms and radial basis functions, *Advances in Computational Mathematics* 40 (2).
- [12] T. Hangelbroek, F. J. Narcowich, C. Rieger, J. D. Ward, Direct and inverse results on bounded domains for meshless methods via localized bases on manifolds, in: J. Dick, F. Kuo, H. Wozniakowski (eds.), *Contemporary Computational Mathematics - A Celebration of the 80th Birthday of Ian Sloan*, Springer, Cham, 2018.
- [13] A. Hussain, S. Haq, M. Uddin, Numerical solution of klein–gordon and sine-Gordon equations by meshless method of lines, *Eng. Anal. Bound. Elem.* 37 (11) (2013) 1351–1366.
- [14] L. Ling, A fast block-greedy algorithm for quasi-optimal meshless trial subspace selection, *SIAM J. Sci. Comput.* 38 (2) (2016) A1224–A1250.
- [15] T. Maerz, C. B. Macdonald, Calculus on surfaces with general closest point functions, *SIAM J. Numer. Anal.* 50 (6) (2012) 3303–3328.
- [16] E. Marchandise, C. Piret, J.-F. Remacle, CAD and mesh repair with radial basis functions, *Journal of Computational Physics* 231 (5) (2012) 2376–2387.
- [17] B. Matérn, *Spatial variation*, vol. 36, Springer Science & Business Media, 2013.
- [18] F. J. Narcowich, X. Sun, J. D. Ward, Approximation power of RBFs and their associated SBFs: A connection, *Adv. Comput. Math.* 27 (1) (2007) 107–124.
- [19] C. Piret, The orthogonal gradients method: A radial basis functions method for solving partial differential equations on arbitrary surfaces, *J. Comput. Phys.* 231 (14) (2012) 4662–4675.
- [20] R. Platte, T. Driscoll, Eigenvalue stability of radial basis function discretizations for time-dependent problems, *Comput. Math. Appl.* 51 (8) (2006) 1251–1268.
- [21] S. J. Ruuth, B. Merriman, A simple embedding method for solving partial differential equations on surfaces, *J. Comput. Phys.* 227 (3) (2008) 1943–1961.
- [22] R. Schaback, Error estimates and condition numbers for radial basis function interpolation, *Adv. Comput. Math.* 3 (3) (1995) 251–264.
- [23] H. Wendland, Error estimates for interpolation by compactly supported radial basis

functions of minimal degree, *J. Approx. Theory* 93 (2) (1998) 258–272.

- [24] H. Wendland, J. Künemund, Solving partial differential equations on (evolving) surfaces with radial basis functions, *Advances in Computational Mathematics* 46 (4).